第 29 卷第 7 期
2013 年 7 月

无 机 化 学 学 报
CHINESE JOURNAL OF INORGANIC CHEMISTRY

Vol.29 No.7
1471-1479

# 基于 1,1′-二苯乙炔-3,3′,5,5′-四羧酸微孔铜配位聚合物的合成和气体吸附性质

胡云霞[1,2] 章文伟*,[1] 王立锋[1,3] 白俊峰*,[1]

([1]配位化学国家重点实验室,南京大学化学化工学院,南京 210093)

([2]新疆凝聚态相变与微结构实验室,伊犁师范学院化学与生物科学学院,伊犁 835000)

([3]南京工业大学应用化学系,南京 210009)

**摘要**: 本文报道了配合物$[Cu_2(EBTC)(H_2O)_2]\cdot 8H_2O\cdot DMF\cdot DMSO$(**1**,EBTC=1,1′-二苯乙炔-3,3′,5,5′-四羧酸根;DMF=*N*,*N*-二甲基甲酰胺;DMSO=二甲基亚砜)的合成、晶体结构和吸附性质。**1** 拥有内径为 0.85 nm 和 0.85 nm×2.15 nm 的两种孔洞,分别被 6 个和 12 个四羧酸根桥联的$[Cu_2(CO_2)_4]$螺旋桨式结构围绕,并被 EBTC 连接成三维超分子结构,该结构拥有可容纳溶剂分子的一维孔道。**1** 为(3,4)-连接的 fof(sqc1575)拓扑结构,具有非常大的孔体积,其值高达单位晶胞体积的 72.8%。去除溶剂分子后的 **1a** 表现出永久孔性,其 Langmuir 表面积为 2844 $m^2\cdot g^{-1}$,BET 表面积为 1 852 $m^2\cdot g^{-1}$。它对 $H_2$、$CO_2$、$CH_4$ 和 $C_2H_2$ 具有可观的气体吸附量和相对较高的吸附焓。特别是,在迄今所有已报道的孔性金属–有机材料中,**1a** 在 273 K、$1.0\times10^5$ Pa 下,表现出最高的乙炔吸附量(252 $cm^3\cdot g^{-1}$)和很高的吸附焓(吸附量为 1 $mmol\cdot g^{-1}$ 时的吸附焓为 34.5 $kJ\cdot mol^{-1}$)。

**关键词**: 微孔金属–有机框架; 溶剂热合成; 晶体结构; 吸附性质

**中图分类号**: O614.121 **文献标识码**: A **文章编号**: 1001-4861(2013)07-1471-09

**DOI**:10.3969/j.issn.1001-4861.2013.00.200

# Synthesis and Gas Sorption Properties of Cupric Microporous Metal-Organic Framework Based on 1,1′-Ethynebenzene-3,3′,5,5′-tetracarboxylate

HU Yun-Xia[1,2] ZHANG Wen-Wei*,[1] WANG Li-Feng[1,3] BAI Jun-Feng*,[1]

([1]*State Key Laboratory of Coordination Chemistry, School of Chemistry and Chemical Engineering, Nanjing University, Nanjing* 210093, *China*)

([2]*Xinjiang Laboratory of Phase Transitions and Microstructures in Condensed Matters, College of Chemistry and Biological Sciences, Yili Normal University, Yili, Xinjiang* 835000, *China*)

([3]*College of Science, Nanjing University of Technology, Nanjing* 210009, *China*)

**Abstract:** The synthesis, crystal structure, and sorption properties of $[Cu_2(EBTC)(H_2O)_2]\cdot 8H_2O\cdot DMF\cdot DMSO$ (abbreviated as **1**, EBTC=1,1′-ethynebenzene-3,3′,5,5′-tetracarboxylate; DMF=*N*,*N*-dimethyl formamide; DMSO=dimethyl sulfoxide) are reported. **1** features two kinds of cavities with a diameter of 0.85 nm and 0.85×2.15 nm, which are enclosed respectively by six and twelve tetracarboxylate-bridged $[Cu_2(CO_2)_4]$ paddle-wheels and extended by the EBTC linkers into a three-dimensional (3D) supramolecular structure with 1D channels accommodating the solvent molecules. It adopts the (3,4)-c net of fof (sqc 1575) topology, possesses very large solvent accessible pore volume which reaches 72.8% of the unit cell volume. After removal of the solvent molecules, the desolvated **1a** exhibits permanent porosity verified by an $N_2$ sorption isotherm with a Langmuir surface area of 2844 $m^2\cdot g^{-1}$ and

收稿日期:2012-08-07。收修改稿日期:2013-03-17。

国家自然科学基金(No.20771058)、国家自然科学基金创新研究群体(No.20721002)、教育部博士点基金(No.200802840011)、新疆凝聚态相变与微结构实验室开放课题基金(No.XJDX0912-2011-01)资助项目。

*通讯联系人。E-mail:wwzhang@nju.edu.cn,bjufeng@nju.edu.cn

Brunauer-Emmett-Teller (BET) surface area of 1 852 $m^2 \cdot g^{-1}$. It displays significant uptake of gases ($H_2$, $CO_2$, $CH_4$, $C_2H_2$) and relatively high adsorption enthalpies. Especially, it is notable that **1a** exhibits the highest acetylene storage of 252 $cm^3 \cdot g^{-1}$ at 273 K under $1.0\times10^5$ Pa with higher adsorption enthalpy (34.5 $kJ \cdot mol^{-1}$ at the coverage of 1 $mmol \cdot g^{-1}$) among all porous metal-organic materials reported to date. CCDC: 744108.

**Key words:** microporous MOFs; solvothermal synthesis; crystal structure; adsorption property

## 0 Introduction

Porous metal-organic frameworks (MOFs) have attracted much attention due to their specific interest in the creation of nanometer-sized spaces and their potential application in gas storage, separation, catalysis, and drug delivery[1]. Usually, the porosity, stability, and pore shape and size of the MOFs play important roles in their features. Currently pore-surface functionalization and framework flexibility are considered to be the key factors for the next generation of MOFs[2-4]. To functionalize the pore/channel surface, two types of strategies are often used: incorporating coordinatively open metal sites (OMSs) to supply guest-accessible sites[5], and/or introducing organic groups to provide guest-responsive functional organic sites (FOSs)[6], which may introduce shape- and/or size-selectivity toward guest molecules.

Recently, tetracarboxylates, such as 3,3′,5,5′-biphenyltetracarboxylate (BPTC), azoxybenzene-3,3′,5,5′-tetracarboxylate (AOBTC), trans-stilbene-3,3′,5,5′-tetracarboxylate (SBTC), have been often used to construct porous frameworks with various topologies ($pt_3o_4$, boracites, nbo, and pts nets)[5,7-8]. But the coordination chemistry of the following ligand, 1,1′-ethynebenzene-3,3′,5,5′-tetracarboxylate (EBTC), still remains largely unexplored[9]. In this paper, we design EBTC as the organic ligand based on the following considerations: first, ligands containing phenyl rings have been proved favorable for hydrogen and methane adsorption[10]; secondly, the ethynylene spacer group of the ligand is of linear shape geometry, which is anticipated to reduce the steric hindrance in supramolecular assemblies and to promote large pore volumes; thirdly, $\pi$ conjugation between aryl groups and the ethynylene linker may increase the electronic interaction with guest molecules; fourthly, the ethynylene moiety may furthermore allow subsequent modification which is beneficial in respect to specific sites formation for molecular recognition or catalysis[9]; finally, EBTC has multiple bridging moieties, thus a variety of connection modes with metal centers are possible to provide abundant structural motifs[11]. To provide coordinatively unsaturated metal centers, Cu(Ⅱ) is promising since it can display a Jahn-Teller distortion and provide an open metal site by facile removal of the apical coordinated volatile molecules[5a,12]. Therefore, porous $[Cu_2(EBTC)(H_2O)_2]\cdot 8H_2O\cdot DMF\cdot DMSO$ (**1**) is constructed to study its sorption properties.

## 1 Experimental

### 1.1 Materials and physical measurement

All the starting reagents and solvents were purchased from commercial sources. 1,1′-Ethynebenzene-3,3′,5,5′-tetracarboxylic acid ($H_4EBTC$) was hydrolyzed from 1,1′-ethynebenzene-3,3′,5,5′-tetramethylcarboxylate, which was prepared from dimethyl 5-iodoisophthalate and dimethyl 5-ethynylisophthalate according to the previously published methods [13-14]. Elemental analyses (C, H and N) were performed on a Perkin-Elmer 240C elemental analyzer. The IR spectra were obtained as KBr disks on a VECTOR 22 spectrometer. Thermal analyses were performed on a TGA V5.1A Dupont 2100 instrument from room temperature to 700 ℃ with a heating rate of 10 ℃·$min^{-1}$ in nitrogen environment. Powder X-ray diffraction (PXRD) data were recorded on a Shimadzu XRD-6000 diffractometer with Cu $K\alpha$ ($\lambda$=0.154 056 nm) radiation at room temperature with a scan speed of 5°·$min^{-1}$ and a step size of 0.02° in $2\theta$.

### 1.2 Preparations

Complex $[Cu_2(EBTC)(H_2O)_2]\cdot 8H_2O\cdot DMF\cdot DMSO$

(**1**) was prepared and characterized as described previously[14]. $H_4EBTC$ (5.0 mg, 0.014 mmol), $Cu(NO_3)_2 \cdot 3H_2O$ (15 mg, 0.06 mmol), DMF (0.2 mL), DMSO (0.2 mL) and $HNO_3$ (0.060 mL, 1.0 mol·L$^{-1}$ in DMF) were placed in a 8 mL glass vial, which was sealed and heated to 65 ℃ for 24 h, and then cooled to room temperature. The greenish-blue block-shaped crystals formed were collected and air-dried (6.3 mg, 55.20% based on $H_4EBTC$). Elemental Analysis Calcd.(%) for $[Cu_2(EBTC)(H_2O)_2]\cdot 8H_2O\cdot DMF\cdot DMSO$: C 34.16, H 4.86, N 1.73. Found(%): C 33.80, H 5.02, N 1.42. IR (cm$^{-1}$): 3 419(br), 3 077(w), 3 002(w), 2 917(w), 1 706 (w), 1 633(s), 1 567(s), 1 430(vs), 1 375(vs), 1 257(w), 1 193(w), 1 106(w), 1 018(m), 950(w), 775(m), 727(m), 678(w), 628(w).

### 1.3 X-ray crystallography

Single crystal X-ray diffraction data of **1** were collected at 293(2) K on a Bruker SMART APEX CCD area-detector diffractometer using graphite-monochromated Mo $K\alpha$ radiation. The structure was solved by direct method and subsequent difference Fourier syntheses, and refined using the SHELXTL software package. The H atoms on the ligands were placed in idealized positions and refined using a riding model. The H atoms of the coordinated $H_2O$ molecules could not be located, but are included in the formula. The unit cell includes a large region of disordered solvent molecules, which could not be modeled as discrete atomic sites. We employed PLATON/SQUEEZE to calculate the diffraction contribution of the solvent molecules and, thereby, to produce a set of solvent-free diffraction intensities[15]. Main data of collection and refinement details of **1** are summarized in Table 1. Selected bond lengths and angles are listed in Table 2.

CCDC: 744108.

## 2 Results and discussion

### 2.1 Structural description

**1** crystallizes in the $R\bar{3}m$ space group with one-half copper atom, one-forth EBTC ligand and one-half coordinated water molecule for the framework in the asymmetric unit (Fig.1). In its crystal, besides a coordinated terminal water molecule in the axial position, each Cu atom coordinates to four carboxylate oxygen atoms from four different EBTC ligands to

**Table 1　Crystal data and structure refinement for 1**

| | | | |
|---|---|---|---|
| Empirical formula | $C_{18}H_{10}O_{10}Cu_2$ | $\gamma$ / (°) | 120 |
| Formula weight | 513.34 | Volume / nm$^3$ | 9.935 3(14) |
| Temperature / K | 293 | $Z$ | 9 |
| Wavelength / nm | 0.071 073 | $F$(000) | 2 304 |
| Crystal system | Trigonal | Crystal size / mm | 0.26×0.26×0.24 |
| Space group | $R\bar{3}m$ | $\theta$ range for data collection / (°) | 1.77 to 28.33° |
| $a$ / nm | 1.868 44(11) | Goodness-of-fit on $F^2$ | 1.088 |
| $b$ / nm | 1.868 44(11) | Final $R$ indices ($I>2\sigma(I)$) | $R_1$=0.047 2, $wR_2$=0.107 7 |
| $c$ / nm | 3.286 2(4) | | |

**Table 2　Selected bond lengths (nm) and angles (°) for 1**

| | | | | | |
|---|---|---|---|---|---|
| Cu1-O2$^{\#1}$ | 0.195 2(3) | Cu1-O1 | 0.196 3(3) | Cu1-O3 | 0.214 9(4) |
| Cu1-O2$^{\#2}$ | 0.195 2(3) | Cu1-O1$^{\#3}$ | 0.196 2(3) | O2-Cu1$^{\#2}$ | 0.195 2(3) |
| C4-C4$^{\#4}$ | 0.117 3(11) | | | | |
| | | | | | |
| O2$^{\#1}$-Cu1-O2$^{\#2}$ | 88.87(18) | O2$^{\#2}$-Cu1-O1$^{\#3}$ | 90.59(12) | O2$^{\#2}$-Cu1-O3 | 94.97(14) |
| O2$^{\#1}$-Cu1-O1 | 90.59(12) | O1-Cu1-O1$^{\#3}$ | 87.59(17) | O1-Cu1-O3 | 96.67(14) |
| O2$^{\#2}$-Cu1-O1 | 168.36(12) | O2$^{\#1}$-Cu1-O3 | 94.97(14) | O1$^{\#3}$-Cu1-O3 | 96.66(14) |
| O2$^{\#1}$-Cu1-O1$^{\#3}$ | 168.36(12) | | | | |

Symmetry codes: $^{\#1}$ $x-y+2/3$, $-y+4/3$, $-z+1/3$; $^{\#2}$ $-x-1/3$, $-y+4/3$, $-z+1/3$; $^{\#3}$ $-x+y-1$, $y$, $z$; $^{\#4}$ $-x$, $-y+1$, $-z$.

form a kind of relatively regular $[Cu_2(CO_2)_4]$ paddle-wheels that are shown in Fig.1. The Cu-O-O-Cu torsion angle is 0.878 degree. The ethynylene bond of the EBTC ligand in **1** (C4-C4$^{\#4}$=0.117 3(11) nm, ∠C3-C4-C4$^{\#4}$=178.1 (12)°) is a little deviated from linearity. The two phenyl rings in it keep coplanar (the dihedral angle of them is zero). The dihedral angles between the carboxylate group and its adjacent phenyl ring are all 6.345°.

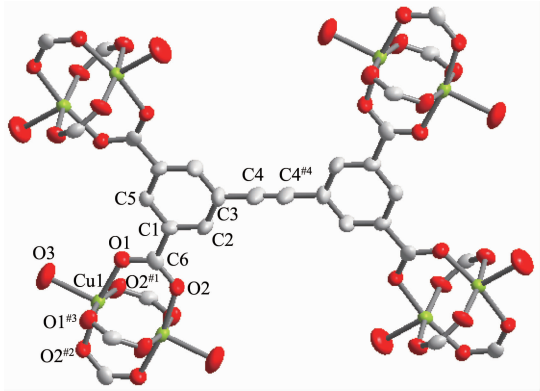


Hydrogen atoms are omitted for clarity; Symmetry codes: $^{\#1}$ $x-y+2/3$, $-y+4/3$, $-z+1/3$; $^{\#2}$ $-x-1/3$, $-y+4/3$, $-z+1/3$; $^{\#3}$ $-x+y-1$, $y$, $z$; $^{\#4}$ $y$, $1+x$, $-z$; Color scheme: Cu, green; C, gray; O, red

Fig.1 Single crystal X-ray structure of **1** showing $Cu_2(CO_2)_4$ and EBTC SBUs with thermal ellipsoids at 50% probability

Like MOF-505, NOTT-101 and some other compounds[16], each EBTC ligand in **1** is linked to four copper paddlewheels via the bridging carboxylate groups. In this kind of 3D framework formed by the interconnected copper paddlewheel secondary building units (SBUs) and EBTC ligands, there exists one type of infinite channel along the *c* axis with window dimensions of 0.37 nm×0.37 nm (Fig.2a, point to point and not including van der Waals radii and coordination water). It is hydrophilic since the water molecules coordinated to the copper centers are pointed inside these channels. Moreover, the framework consists of two different types of open cages which are alternately stacked with each other along this pore axis (Fig.2b): the small cage is encapsulated by six $Cu_2(COO)_4$ clusters with a pore diameter of 0.85 nm, and the large irregular elongated cage is about 0.85 nm×2.15 nm surrounded by twelve $Cu_2(COO)_4$ clusters (Fig.2c). Noticeably, the two different diameter cages have the same pore windows characteristic of three $Cu_2(COO)_4$ clusters as the channels. After the framework is activated without the coordinated water and some other guest solvent molecules (**1a**), the pore walls are formed by the hydrophobic parts of the ligand molecules with open metal sites (OMSs) and special C≡C bonds. Different from the OMSs′ nonlinear arrangement in MOF-505 with similar structure, the open $Cu^{2+}$ sites in **1** are oppositely aligned (Fig.3). It will be mentioned below that the characteristic porous structures of **1**, such as pore window sites, the open $Cu^{2+}$ sites, the arrangement of the OMSs, and the C≡C bonds in the MOFs, are expected to play crucial roles in their gas adsorption. The theoretical solvent accessible void is 72.8% in the unit cell based on a

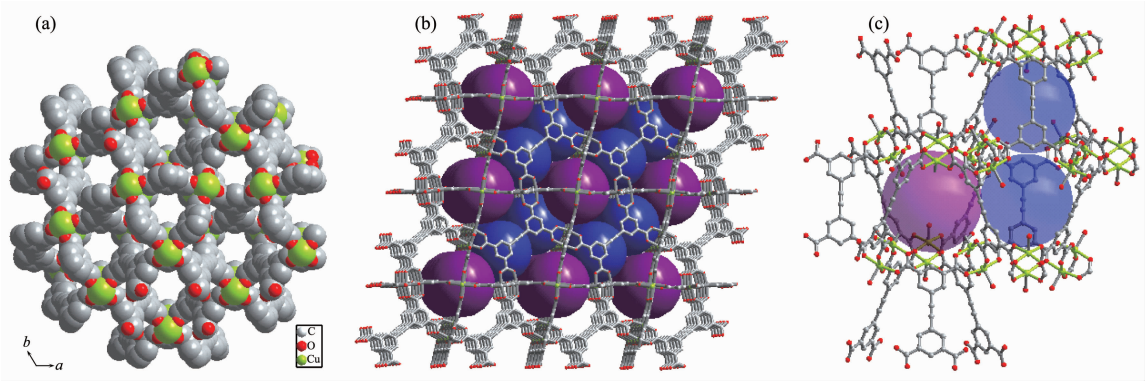


In (c): (i) small cage can be occupied by a violet sphere about 0.85 nm in diameter and (ii) large irregular elongated cage about 0.85×2.15 nm can be occupied by two blue spheres. Color scheme: Cu, green; C, gray; O, red

Fig.2 (a) X-ray single crystal structure of **1a** exhibiting one type of infinite channel along the *c* axis; (b) **1a** showing two types of cages alternately stacked with each other; (c) Two types of cages in **1a**

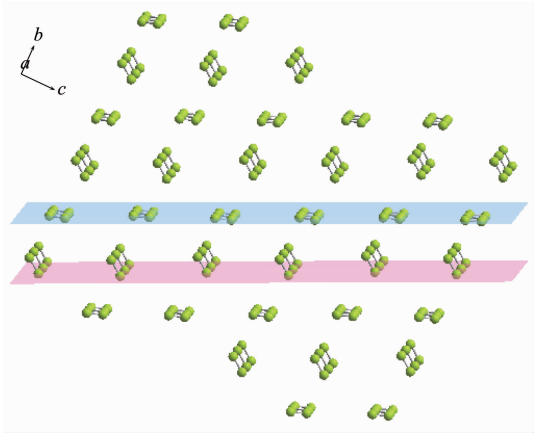


Fig.3　X-ray single crystal structure of **1** exhibiting the open $Cu^{2+}$ sites oppositely aligned

PLATON calculation.

As for the topology of **1**, two kinds of SBUs, the inorganic [$Cu_2(CO_2)_4$] paddlewheel and the organic EBTC unit, are contributed to it, just like MOF-505, IZE-1 and some other complexes[11b,16]. When considering both the dinuclear $Cu_2(CO_2)_4$ SBU and the EBTC ligand as planar 4-c nodes, **1** would adopt the cubic 4-c nbo net[11b,16,17a]. However, preferable description could be obtained as below: the $Cu_2(CO_2)_4$ paddlewheel can be served as planar 4-c node which is defined by the carboxylate carbon atoms, and the organic EBTC linker can be considered as two 3-c nodes centered between two phenyl rings (Fig.4a), leading to two different (3,4)-c nets[11b,17a-c]. In this view, **1** is observed as (3,4)-c fof net (alternative name sqc1575), with point symbol of $(6.8^2)_2(6^2.8^2.10^2)$ and vertex symbol of $(6.8_2.8_2)(6.6.8_2.8_2.10_2.10_2)$ (Fig.4b)[11b,17].

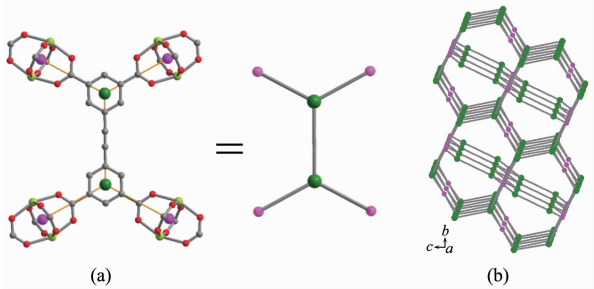


Color scheme: Cu, green; C, gray; O, red. Hydrogen atoms are omitted for clarity

Fig.4　Illustration of topology of **1**: (a) simplification of the organic EBTC linker (two 3-connected nodes, dark green balls) and the inorganic $Cu_2(CO_2)_4$ paddlewheels (4-connected node, pink balls), (b) topological view of 1, the (3,4)-c fof (sqc1575) net

Powder X-ray diffraction (PXRD) patterns and thermal gravimetric analysis (TGA) were used to evaluate the framework stability under solvent-exchange conditions. PXRD reveals the same pattern of intense diffraction lines in each of the simulated, as-synthesized, and methanol, ethanol, acetone exchanged materials (Fig.5). This indicates that **1** is stable upon solvent exchange. However, upon desolvation of the methanol exchanged material, decreased diffraction intensities and broadened reflections were observed in the PXRD pattern. This indicates some loss of long-range order but not necessarily loss of porosity[5c].

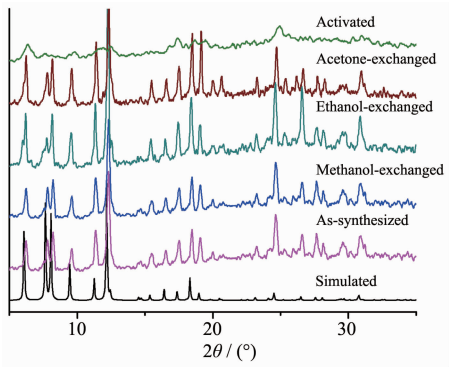


Fig.5　PXRD patterns for **1** at different conditions

TGA data of **1** indicate three consecutive weight loss stages (Fig.6a). The initial weight loss (16.7%) bellow 110 ℃ corresponds to the dehydration of 8 guest water molecules (Calcd. 17.8%) per $Cu_2$EBTC formula unit. This step is followed by an additional weight loss of 23.8% at 110~207 ℃, which corresponds to the liberation of two coordinated water molecules, one guest DMF and one guest DMSO molecules (Calcd. 23.2%) per formula unit. Thus the total weight loss of **1** (all guest solvents in the cage and the coordinated water with $Cu^{2+}$) from room temperature to 207 ℃ is 40.5% (Calcd. 41.0%). It is comparable to the data of 41.5% weight loss from room temperature to 100 ℃ after dipping **1** in methanol for several times (Fig.6b, corresponding to 11.5 methanol molecules per $Cu_2$EBTC formula unit), which suggests that all the guest solvents and the coordinated water in **1** have been completely exchanged by methanol. Apparently methanol exchanged **1** is stable up to 300 ℃ from its

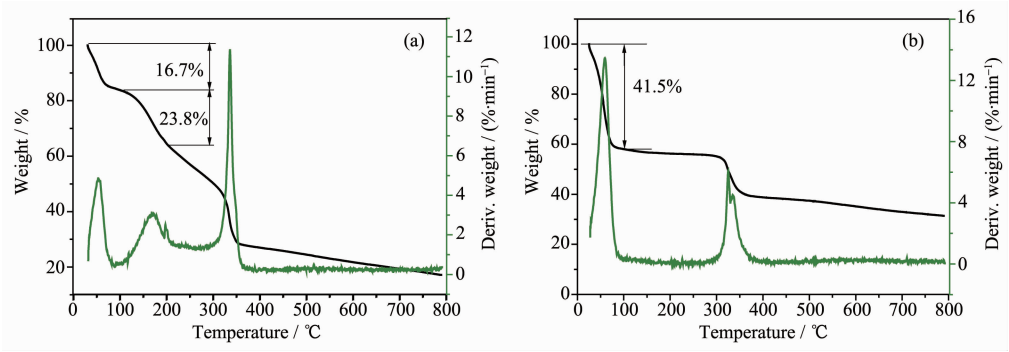


Fig.6 TGA data of **1**: as-synthesized (a) and methanol exchanged (b)

TGA curve. It is in accordance with the stability of free $H_4$EBTC which decomposes at 300 ℃.

## 2.2 Adsorption studies

As described above, it is obvious that the desolvated **1a** has narrow channels with accessible metal sites and hydrophobic pore walls with C≡C bonds. Owing to its interesting structural and functional features, we explored $N_2$, $H_2$, $CO_2$, $CH_4$ and $C_2H_2$ uptake on it. The sample activation (about 100 mg of methanol-exchanged **1** (6~8 times)) occurred at elevated temperature (393 K) in a dynamic vacuum overnight until the outgas rate was less than 4 mmHg·min$^{-1}$ to form anhydrous **1a**. We obtained the gas sorption isotherms using a Micromeritics ASAP 2020 system to measure the change in volume of samples suspended within a glass enclosure under a chosen gas atmosphere. The sorption isotherms for desolvated **1a** are shown in Fig.7. Nitrogen sorption clearly shows reversible type-Ⅰ isotherm with homogenous pores, indicating permanent porosity after removal of solvent from the crystalline samples. The BET surface area and Langmuir surface for desolvated **1a** are estimated as 1 852 and 2 880 $m^2·g^{-1}$, respectively. The theoretical pore volume is 1.014 $cm^3·g^{-1}$, while the experimental pore volume from *t*-plot is 0.96 $cm^3·g^{-1}$. The largest pore size is 0.68 nm from Horvath-Kawazoe Differential Pore Volume Plot.

Under lower pressure, the $H_2$ sorption isotherm of **1a** reveals an uptake of 286 $cm^3·g^{-1}$ (2.58wt%, 77 K) at $1.0\times10^5$ Pa, which is within the adsorption values of analogous compound MOF-505, NOTT-101, NOTT-102 [16a,b] constructed from biphenyl-, terphenyl-, and quaterphenyl-tetracarboxylate and PCN-46[16c] built from 5,5′-(buta-1,3-diyne-1,4-diyl)diisophthalate linker with similar topology. Moreover, the $H_2$ adsorption is still far from saturation for **1a** under low pressure, indicating that their $H_2$ storage capacity is dominated by the affinity between $H_2$ molecules and the frameworks. When the $H_2$ pressure is increased, 1a adsorbs additional $H_2$ gas, until saturation is nearly reached at $1.0\times10^6$ Pa. Above this pressure, it has very little potential to adsorb more $H_2$. The highest adsorption of $H_2$ by **1a** is about 561 $cm^3·g^{-1}$ (5.01wt%, 77 K) recorded at $2.0\times10^6$ Pa, which is also within the uptakes of the above analogous compounds with different ligand length. Compare the $H_2$ uptakes of MOF-505, **1a**,

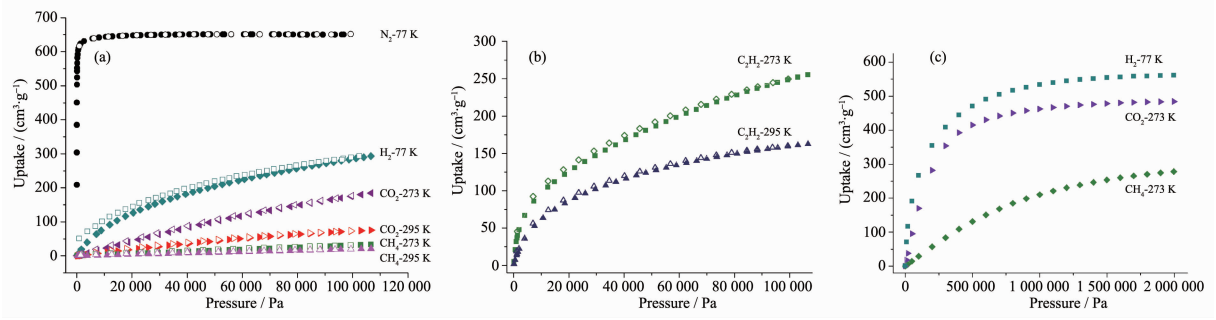


Filled and open circles represent adsorption and desorption branches, respectively

Fig.7 Low pressure (a and b) and high pressure (c) gas sorption isotherms of **1a** at different temperatures

NOTT-101, PCN-46 and NOTT-102, it is interesting to find that, with ligand length increasing, the adsorption value at high pressure increases while that under low pressure decreases. This further confirms the theoretical studies on porous MOFs that higher gravimetric $H_2$ uptake at high pressure would be got with higher specific surface area[18], and it also suggests that the enhancement of adsorption in smaller pores at low pressures is mainly controlled by the hydrogen affinity towards the framework, which indicates that an optimum pore size may exist to maximize $H_2$ uptake[16].

The same sorption behavior is observed for $CO_2$. The isotherms are reversible and show no hysteresis upon desorption of gases from the pores under low pressure. Its carbon dioxide capacity levels are 178 $cm^3 \cdot g^{-1}$ (35wt%, 273 K) and 74 $cm^3 \cdot g^{-1}$ (15wt%, 295 K) at atmospheric pressure, which are comparable to those of isomorphic MOFs of MOF-505 and SNU-5[5a]. It is evident that the adsorption is also still far from saturation for **1a**, indicating that the $CO_2$ storage capacity is also dominated by the affinity between the adsorbed molecules and the frameworks. High-pressure carbon dioxide sorption measurement shows that the total adsorption capacities of $CO_2$ in **1a** can be up to 484 $cm^3 \cdot g^{-1}$ (373 $L \cdot L^{-1}$, 95wt%) at 273 K and $2.0\times10^6$ Pa, that′s to say, 1 L of **1a** can hold 373 L of $CO_2$. The coverage-dependent adsorption enthalpies of **1a** for $CO_2$ were calculated based on the virial method[19], a well established and reliable methodology, from fits of their adsorption isotherms at 273 and 295 K under low pressure. As shown in Fig.8, **1a** exhibits adsorption enthalpies of $CO_2$ with 24.7~25.4 $kJ \cdot mol^{-1}$, depending on the degree of $CO_2$ loading.

The methane sorption isotherm of **1a** reveals an uptake of 31 $cm^3 \cdot g^{-1}$ (23.9 $cm^3 \cdot cm^{-3}$, 273 K) and 20 $cm^3 \cdot g^{-1}$ (15.4 $cm^3 \cdot cm^{-3}$, 295 K) at atmospheric pressure, which are still far from saturation. As the pressure is increased, the adsorption of methane occurs with a gradually increasing uptake and reaches an adsorbed amount close to 278 $cm^3 \cdot g^{-1}$ (215 $L \cdot L^{-1}$) up to $2.0\times10^6$ Pa at 273 K, which can be compared with PCN-14 (248 $L \cdot L^{-1}$ at 270 K and $2.0\times10^6$ Pa)[20], the reported

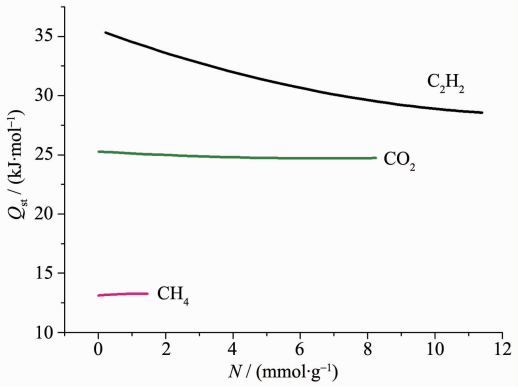


Fig.8　Coverage dependencies of the adsorption enthalpies for $C_2H_2$, $CO_2$ and $CH_4$ in **1a** calculated from fits of their 273 and 295 K isotherms

experimental highest methane sorption material in MOFs to date. Moreover, it is worth noting that **1a** displays a small but unambiguous hysteresis for $CH_4$ sorption isotherms under low pressure. It may be due to the reason that methane is not able to easily leave the cage structure within **1a** since the kinetics diameter of methane (0.375 8 nm) is a little larger than the pore window (0.37 nm).

The adsorption enthalpy of $CH_4$ for **1a** is about 13.2 $kJ \cdot mol^{-1}$ at the coverage of 1 $mmol \cdot g^{-1}$. Obviously, it is lower than that of PCN-14 (25 $kJ \cdot mol^{-1}$ at the coverage of 1 $mmol \cdot g^{-1}$), but it is also comparable to the values of the most interesting MOF structures which reported to be in the range of 12~15.5 $kJ \cdot mol^{-1}$ [21].

Compare the adsorption data of $CO_2$ and $CH_4$ given above, it can be seen that the $CO_2$ uptake is higher than that of $CH_4$ at similar conditions, which suggests a stronger interaction between the framework and $CO_2$ molecules probably arising from the C–H$\cdots\pi$ and (or) $\pi$-$\pi$ interactions between EBTC groups and carbon dioxide guests in **1a**[22].

Although the volume of $C_2H_2$ (112.20 $cm^3 \cdot mol^{-1}$) is larger than $CH_4$ (98.6 $cm^3 \cdot mol^{-1}$)[23], but the kinetics diameter of $C_2H_2$ (0.33 nm) is smaller than $CH_4$ (0.375 8 nm), and it is also smaller than the pore window (0.37 nm) of **1a**. So the sorption behavior of $C_2H_2$ is different from that of $CH_4$. The isotherms are reversible and show no hysteresis upon desorption of acetylene from the pores under low pressure (Fig.7b). **1a** takes

up 160 $cm^3 \cdot g^{-1}$ and 252 $cm^3 \cdot g^{-1}$ $C_2H_2$ at 295 K and 273 K under $1.0\times10^5$ Pa, respectively. Its adsorption enthalpies are in the range of 28.5~35.2 $kJ \cdot mol^{-1}$ at different coverage. Remarkably, it exhibits the highest $C_2H_2$ storage capacity at 273 K and $1.0\times10^5$ Pa, and its $C_2H_2$ adsorption enthalpies are higher than any other data of the MOFs (HKUST-1, MOF-505, MOF-508, MIL-53, etc.) at similar coverage ever reported to date[24a]. All above indicate that stronger interactions may exist between acetylene molecules and pore surfaces in **1a**. On the one hand, just as HKUST-1and MOF-505 with similar structures, **1a** also has open $Cu^{2+}$ sites, the strongest binding sites to adsorb acetylene molecules verified by neutron powder diffraction studies[24a], which enhance their interactions with acetylene molecules[24b] and contribute to the significantly larger amount of acetylene adsorption. Secondly, **1a** has suitable pore window size, and the entrance window of the small cage is established to be the second strongest binding site of acetylene[24a], this may also give rise to higher acetylene storage capacity. Thirdly, the different arrangement of the open $Cu^{2+}$ metal sites and their orientation with respect to each other in **1a** may play an important role in its higher acetylene uptake comparable to that of HKUST-1 and MOF-505. It is known from the crystal structure that the open $Cu^{2+}$ sites in MOF-505 deviate from the linearity, while those in 1a are oppositely aligned, as a result, it may lead to stronger interactions with acetylene guest molecules in **1a** as established in similar MOFs for hydorgen storage[24c]. And finally, the C≡C bonds within the **1a** MOFs might also enhance their interactions with acetylene through weak $\pi$-$\pi$ interactions. Therefore, the dense open metal sites and their appropriate arrangement, suitable pore window sites, together with the weak $\pi$-$\pi$ interactions between the -C≡C- bonds and acetylene, are cooperatively responsible for the strong interactions of acetylene molecules with **1a** MOFs, and hence, significantly high acetylene storage are obtained.

## 3 Conclusions

In conclusion, we have successfully synthesized and characterized the 3D porous metal-organic frameworks $[Cu_2(EBTC)(H_2O)_2]\cdot8H_2O\cdot DMF\cdot DMSO$ (**1**) containing -C≡C- bond with fof (sqc1575) type topology. The $N_2$ sorption measurements showed that the activated **1a** has a permanent porosity with higher surface area. Volumetric measurements of **1a** reveal that it exhibits relatively high adsorption ability towards $H_2$, $CO_2$, $CH_4$ and $C_2H_2$. The extraordinarily high acetylene uptake indicates that rational design of the MOFs with dense open metal sites, suitable pore sizes and specific binding sites, such as adding -C≡C- to the ligand, can increase their strong recognition of adsorbed molecules. Such criteria may be taken into account in the design of new hybrid solids with improved storage properties.

**Acknowledgements:** This work was supported by the NSFC (No. 20771058), the Science Foundation of Innovative Research Team of NSFC (No. 20721002), the Specialized Research Fund for the Doctoral Program of the Ministry of Education of China (No. 200802840011), and the Opening Project of Xinjiang Laboratory of Phase Transitions and Microstructures of Condensed Matters (No. XJDX0912-2011-01). We also gratefully appreciated Dr. Shengchang Xiang and Prof. Banglin Chen for their kind help.

## References:

[1] (a)Zaworotko M J. *Nature Chemistry*, **2009**,**1**:267-268
(b)Zaworotko M. *J. Nature*, **2009**,**451**:410-411
(c)Ma S, Sun D, Yuan D, et al. *J. Am. Chem. Soc.*, **2009**,**131**:6445-6451
(d)Férey G, Mellot-Draznieks C, Serre C, et al. *Science*, **2005**, **309**:2040-2042
(e)Zhang J P, Chen X M. *J. Am. Chem. Soc.*, **2009**,**131**:5516-5521

[2] (a)Kitagawa S, Kitaura R, Noro I S. *Angew. Chem. Int. Ed.*, **2004**,**43**:2334-2375
(b)Zhang J P, Chen X M. *J. Am. Chem. Soc.*, **2008**,**130**:6010-6017

[3] (a)Férey G. *Chem. Soc. Rev.*, **2008**,**37**:191-214
(b)Kitagawa S, Matsuda R. *Coord. Chem. Rev.*, **2007**,**251**:2490-2509
(c)Kepert C J. *Chem. Commun.*, **2006**,**7**:695-700
(d)Fletcher A J, Thomas K M, Rosseinsky M J. *J. Solid State Chem.*, **2005**,**78**:2491-2510

[4] (a)Ghosh S K, Zhang J P, Kitagawa S. *Angew. Chem. Int. Ed.*, **2007**,**46**:7965-7968
(b)Serre C, Mellot-Draznieks C, Surble S, et al. *Science*, **2007**,**315**:1828-1831
(c)Kubota Y, Takata M, Matsuda R, et al. *Angew. Chem. Int. Ed.*, **2006**,**45**:4932-4936

[5] (a)Lee Y G, Moon H R, Cheon Y E et al. *Angew. Chem. Int. Ed.*, **2008**,**47**:7741-7745
(b)Zhang J P, Horike S, Kitagawa S. *Angew. Chem. Int. Ed.*, **2007**,**46**:889-892
(c)Chen B L, Ockwig N W, Millward A R, et al. *Angew. Chem. Int. Ed.*, **2005**,**44**:4745-4749

[6] (a)Horike S, Bureekaew S, Kitagawa S. *Chem. Commun.*, **2008**,**4**:471-473
(b)Hasegawa S, Horike S, Matsuda R, et al. *J. Am. Chem. Soc.*, **2007**,**129**:2607-2614

[7] Lin X, Jia J, Zhao X, et al. *Angew. Chem. Int. Ed.*, **2006**, **118**:7358-7364

[8] Chen B, Ockwig N W, Fronczek F R, et al. *Inorg. Chem.*, **2005**,**44**:181-183

[9] Hausdorf S, Seichter W, Weber E, et al. *Dalton Trans.*, **2009**,**7**:1107-1113

[10]Wang X S, Ma S Q, Rauch K, et al. *Chem. Mater.*, **2008**,**20**: 3145-3152

[11](a)Wang L F, Kang L C, Zhang W W, et al. *Dalton Trans.*, **2011**,**40**:9490-9497
(b)Hu Y X, Ma H B, Zheng B, et al. *Inorg. Chem.*, **2012**,**51**: 7066-7074

[12]Kitagawa S, Noro S I, Nakamura T. *Chem. Commun.*, **2006**, **7**:701-707

[13](a)Thorand S, Krause N. *J. Org. Chem.*, **1998**,**63**:8551-8553
(b)Sonogashira K. *J. Organomet. Chem.*, **2002**,**653**:46-49
(c)Bodwell G J, Miller D O, Vermeij R J. *Org. Lett.*, **2001**,**3**: 2093-2096

[14]Hu Y X, Xiang S C, Zhang W W, et al. *Chem. Commun.*, **2009**,**48**:7551-7553

[15](a)Spek A L. *J. Appl. Crystallogr.*, **2003**,**36**:7-13
(b)Spek A L. *PLATON, A Multipurpose Crystallographic Tool*, Utrecht University, The Netherlands, **2006**. available via http://www.cryst.chem.uu.nl/platon (for Unix) and http://www.chem.gla.ac.uk/Blouis/software/platon/ (for MS Windows)

[16](a)Lin X, Jia J, Zhao X, et al. *Angew. Chem. Int. Ed.*, **2006**, **45**:7358-7364
(b)Lin X, Telepeni I, Blake A J, et al. *J. Am. Chem. Soc.*, **2009**,**131**:2159-2171
(c)Zhao D, Yuan D, Yakovenko A, et al. *Chem. Commun.*, **2010**,**46**:4196-4198

[17](a)Sun D, Ma S, Simmons J M, et al. *Chem. Commun.*, **2010**, **46**:1329-1331
(b)O′Keeffe M, Yaghi O M. *Chem. Rev.*, **2012**,**112**:675-702
(c)Alexandrov E V, Blatov V A, Kochetkov A V, et al. *CrystEngComm*, **2011**,**13**:3947-3958
(d)O′Keeffe M, Peskov M A, Ramsden, S J, et al. *Acc. Chem. Res.*, **2008**,**41**:1782-1789
(e)Ramsden S J, Robins V, Hyde S T, *Acta Crystallogr. Sect. A*: *Found. Crystallogr.*, **2009**,**65**:81-108
(f)Blatov V A, O′Keeffe M, Proserpio D M. *CrystEngComm*, **2010**,**12**:44-48

[18](a)Walton K S, Snurr R Q. *J. Am. Chem. Soc.*, **2007**,**129**: 8552-8556
(b)Han S S, Goddard W A. *J. Phys. Chem. C*, **2008**,**112**: 13431-13436

[19]Rowsell J L C, Yaghi O M. *J. Am. Chem. Soc.*, **2006**,**128**: 1304-1315

[20](a)Ma S Q, Sun D F, Simmons J M, et al. *J. Am. Chem. Soc.*, **2008**,**130**:1012-1016
(b)Wu H, Zhou W, Yildirim T. *J. Am. Chem. Soc.*, **2009**, **131**:4995-5000

[21]Senkovska I, Kaskel S. *Micropor. Mesopor. Mat.*, **2008**,**112**: 108-115

[22]Busker M, Hber T, Nispel M, et al. *Angew. Chem. Int. Ed.*, **2008**,**47**:10094-10097

[23]Li J R, Kuppler R J, Zhou H C. *Chem. Soc. Rev.*, **2009**,**38**: 1477-1504

[24](a)Xiang S C, Zhou W, Gallegos J M, et al. *J. Am. Chem. Soc.*, **2009**,**131**:12415-12419
(b)Reisinger A, Trapp N, Krossing I, et al. *Angew. Chem. Int. Ed.*, **2007**,**46**:8295-8298
(c)Wang X S, Ma S, Forster P M, et al. *Angew. Chem. Int. Ed.*, 2008,**47**:7263-7266